https://doi.org/10.5194/egusphere-2025-787
Preprint. Discussion started: 6 March 2025

Water Vapor Content Retrieval Under Cloudy Sky Conditions from SWIR Satellite Measurements in the Context of C^{3}IEL Space Mission Project

Raphaël Peroni[1,+], Guillaume Penide[1], Céline Cornet[1], Olivier Pujol[1], and Clémence Pierangelo[2]

[1]Univ. Lille, CNRS, UMR 8518 - LOA - Laboratoire d'Optique Atmosphérique, F-59000 Lille, France
[2]Centre National d'Etudes Spatiales (CNES), 18 avenue Edouard Belin, 31401 TOULOUSE Cedex 9, France
[+]Now at Department of Earth and Atmospheric Sciences, Université du Québec à Montréal, Montreal, Canada

Correspondence: Céline Cornet (celine.cornet@univ-lille.fr)

Abstract. A retrieval algorithm of integrated water vapor content above cloud, using shortwave infrared observations, is developed and evaluated through idealized and realistic atmospheric profiles. Water vapor plays a crucial role in cloud formation and development, particularly those resulting from convective processes. The resulting convective cloud locally influences the spatio-temporal variability of atmospheric water vapor content, through exchanges between cloud and its immediate environment. Therefore, a better understanding of the water vapor content above and around clouds is necessary to improve our comprehension of interactions between water vapor and cloud to better constrain Large-Eddy Simulations (LES) and numerical weather forecasting models. The developed algorithm is part of the Cluster for Cloud evolution, ClImatE and Lightning, C^{3}IEL space mission project. This mission, scheduled for early 2028, aims to enhance our knowledge of the 3D convective cloud development velocities, the electrical activity associated with convective systems, and the water vapor content above and around the cloud. The retrieval algorithm presented in this study is achieved through a Bayesian probabilistic approach, the optimal estimation method. The atmosphere is assumed to be composed of homogeneous plane-parallel layers, and synthetic radiance datasets were generated to test the developed retrieval algorithm. The feasibility of retrieving the integrated water vapor content above the cloud over the ocean from SWIR radiances is shown to have, under idealized vertically homogeneous cloud profiles, absolute errors less than $2\ \mathrm{kg.m^{-2}}$ for optically thick clouds or when the integrated water vapor content is below $20\ \mathrm{kg.m^{-2}}$ and less than $1\ \mathrm{kg.m^{-2}}$ for very thick clouds with an optical thickness exceeding 150. Tests using realistic water vapor and cloud extinction profiles that present non-homogeneous vertical distributions show that integrated water vapor content above water type clouds could be retrieved with a Root-Mean-Square Error (RMSE) related to cloud vertical penetration of approximately less than $1\ \mathrm{kg.m^{-2}}$ except for optically thin and low-level clouds (cloud optical thickness less than 50 and cloud top height less than $2\ \mathrm{km}$). For very low water vapor content encountered in the presence of high deep convective clouds, the retrieval algorithm tends to systematically overestimate the retrieved water vapor content due to an overestimation of the cloud extinction profile in the upper part of the cloud in the inversion model.

https://doi.org/10.5194/egusphere-2025-787
Preprint. Discussion started: 6 March 2025

1 Introduction

Clouds play a significant role in Earth's energy balance, as they can induce a positive or negative radiative forcing whose uncertainty is still important (*e.g.,* Stocker et al., 2013; Masson-Delmotte et al., 2021). Depending on their latitude, characteristics, altitude and temperature, their radiative forcing can be different (*e.g.,* Ramanathan et al., 1989; Harrison et al., 1990). In fact, lower tropospheric clouds, which are composed primarily of liquid water, tend to reflect solar radiation at all wavelengths, resulting in a cooling effect (*e.g.,* Fermepin and Bony, 2014), named the parasol effect (*e.g.,* Crutzen and Ramanathan, 2003). In contrast, solar radiation goes through upper thin tropospheric clouds, such as *cirrus* but these thin high clouds absorb thermal radiation from the Earth and re-emit infrared radiation towards space at a lower temperature due to their cold temperature, thereby enhancing the greenhouse effect (*e.g.,* Jensen et al., 1996; McFarquhar et al., 2000; Lee et al., 2009; Schmidt et al., 2010). A more detailed description of *cirrus* type clouds and their effects on the Earth-Atmosphere system can be seen in Lynch (2002). Deep convective clouds combines both effect as they reflect a significant amount of incoming solar radiation back into space and emits infrared radiation at a low temperature due to the high level of their top. It is therefore essential to better understand cloud development in order to accurately assess their radiative impact on the Earth's energy balance. As an example, Bony et al. (2015) address the scientific community with several questions aimed at emphasizing the importance of a better understanding of the role of cloud feedbacks and convective organization on climate, as well as the factors that influence cloud formation.

Cloud formation and development depend on the amount of water vapor available in the atmosphere. Indeed, with regard to the temperature, the saturation vapor pressure can be reached. Water vapor will then condense either on Cloud Condensation Nuclei (CCN) to form new cloud droplets or on Ice Nuclei (IN), to form new ice crystals. The latent heat released during water vapor condensation and cloud formation not only disturbs the thermal structure of the atmosphere (*e.g.,* Trenberth and Smith, 2005; Schneider et al., 2010) but also fuels cloud development through a chain reaction.

In the free troposphere, humidity influences the dynamical development of clouds through entrainment and detrainment processes. Convection processes, in turn, contribute significantly to the redistribution of energy and water vapor in the atmosphere (*e.g.,* Blyth, 1993). Humidity above and around clouds is therefore an essential parameter in the process of cloud development, particularly in the case of convective clouds.

Many spaceborne remote sensing instruments have been developed to retrieve water vapor across various spectral domains. Microwave sounders such as the Sounder for Probing Vertical Profiles of Humidity (SAPHIR) aboard the French-Indian satellite MEGHA-TROPIQUES (*e.g.,* Desbois et al., 2007), or AMSU (the Advanced Microwave Sounding Unit) aboard the NOAA satellite, make it possible to conduct measurements at all weather conditions and provide either humidity profiles or information on total water vapor content at a spatial resolution of $12\ \mathrm{km}$ at nadir for SAPHIR (*e.g.,* Rao et al., 2013), $48\ \mathrm{km}$ at nadir for AMSU-A, and $16\ \mathrm{km}$ for AMSU-B (*e.g.,* Rosenkranz, 2001; Karbou et al., 2005). Humidity profile retrieval in clear sky conditions or above thick clouds are also performed by the Infrared Atmospheric Sounding Interferometer (IASI) instrument operating in the thermal infrared (TIR) with a spatial resolution of $8\ \mathrm{km}$ (*e.g.,* Schlüssel and Goldberg, 2002; Hilton et al., 2012). These instruments give a vertical information on the water vapor content in the atmosphere but their limitation to study

https://doi.org/10.5194/egusphere-2025-787
Preprint. Discussion started: 6 March 2025

cloud and water vapor interactions lies in their low spatial resolutions and not contiguous pixels, which do not allow for precise examination of these interactions.

Near-Infrared (NIR) or Shortwave Infrared (SWIR) imagers allow to derive water vapor content at a better spatial resolution under clear sky conditions through the differential absorption method, either with airborne measurements (*e.g.,* Bouffiès et al., 1997), or from spaceborne sensors such as the POLarization and Directionaly of Earth Reflectance instrument (POLDER: *e.g.,* Vesperini et al., 1999), the Medium Resolution Imaging Spectrometer (MERIS: *e.g.,* Bennartz and Fischer, 2001) or the MODerate resolution Imaging Spectroradiometer (MODIS: *e.g.,* Gao and Kaufman, 2003). All of these retrieval algorithms propose parameterizations that link the Total Column Water Vapor (TCWV), in $\mathrm{kg.m^{-2}}$, to the ratio of NIR or SWIR spectral bands within absorbing and non-absorbing channels. However, in cloudy sky conditions, these parameterizations are no longer sufficient as clouds interact with the measurements. Indeed, in this particular spectral domain, clouds are not transparent to radiation (as it is in the microwave domain). Moreover, as clouds do not act as a perfect reflector, radiation penetrates the cloud and gets scattered, effectively extending the radiation path through the atmosphere and consequently increasing absorption by water vapor or any other absorbing gas. Albert et al. (2001) demonstrates the feasibility of retrieving water vapor content above cloud in the SWIR domain, over various types of surface, and in the presence of low and optically thick clouds, applying the differential absorption method to simulations conducted in the context of the POLDER and MERIS instruments. They demonstrated with simulations that the absorption of solar radiation within a water vapor absorption band is influenced by the "radiation path", modified by the presence of clouds. On one hand, multiple scattering increases the path length traveled by radiation, leading to higher absorption by water vapor and consequently, a higher retrieved water vapor content. On the other hand, the presence of clouds reduces or stops the influence of lower atmospheric layers, resulting in reduced overall absorption (Albert et al., 2001). They conclude that retrieving water vapor above cloud is feasible for high values of cloud optical thickness. By adjusting the path in their method and applying it to POLDER measurements, they report an average root mean square error (RMSE) of $1.8\ \mathrm{kg.m^{-2}}$ over ocean, as compared with radio-sounding data. (Vidot et al., 2009) conducted a feasibility study using an optimal estimation method within the framework of the Orbiting Carbon Observatory (OCO) sensor, quantifying various type of errors to demonstrate the potential for retrieving column-averaged carbon dioxide mixing ratios over liquid water clouds above the ocean. Similarly, (Schepers et al., 2016) used SWIR measurements from the Greenhouse Gas Observing Satellite (GOSAT) to simultaneously retrieve the total columns of methane and carbon dioxide above clouds, along with cloud properties.

In this study, the objective is to retrieve the integrated water vapor content above cloud using SWIR satellite observations with high spatial and temporal resolution over the ocean in the context of the the Cluster for Cloud evolution, ClImatE and Lightning (C^3IEL) mission. The main advantage that can be exploited is the knowledge of the cloud top height retrieved with good accuracy thanks to the CLOUD radiometers (Dandini et al., 2022). Firstly, in section 2, we provide an overview of the study's context, specifically the space mission project C^3IEL that contextualizes our work. Then in section 3, we discuss the method employed in the developed retrieval algorithm. Section 4 shows the sensitivity of the C^3IEL water vapor channels to the integrated water vapor content above cloud (IWV_{AC}). In section 5, the algorithm is tested first under idealized cloudy atmospheric conditions, then under realistic conditions. Finally, section 6 summarizes the main findings and perspectives.

https://doi.org/10.5194/egusphere-2025-787
Preprint. Discussion started: 6 March 2025

2 The C^{3}IEL space mission project

The space mission project named as the Cluster for Cloud evolution, ClImatE and Lightning, C^{3}IEL (Rosenfeld et al., 2022) started in 2016 through a partnership between the French space agency (CNES) and the Israeli Space Agency (ISA). Its primary objective is to explore the dynamical development of convective clouds, including *cumulus congestus* and *cumulonimbus* clouds. This will be achieved by gathering data at high spatial and temporal resolutions, through 11 acquisitions of two simultaneous observations every 20 seconds during a sequence of 200 seconds. C^{3}IEL consist of a pair of satellites operating in tandem, distanced by about 150 km following a sun-synchronous orbit at about 1 : 30 PM local time at the equator. The altitude of the orbit is expecting to be between 600 and 700 km. The underlying measurement principles is represented in figure 1. The viewing angles for each satellite will be approximately $\pm 50\ °$, $-42\ °$, $-32\ °$, $-20\ °$, and $-7\ °$ on each side of the observed scene. Additionally, the first satellite will include a $-55\ °$ angle, while the second satellite will include a $+55\ °$ angle. This strategy of observations will provide (1) the 3D envelope of convective clouds and their vertical/horizontal development velocities (Dandini et al., 2022) using the visible imagers named CLOUD, measuring at 670 nm with a high spatial resolution (20 m at nadir), (2) the associated electrical activity generated by convective processes with the instruments Lightning Optical Imager and Photometers (LOIP) consisting in visible imagers measuring at 777 nm with a spatial resolution of 140 m at nadir and two photometers at 337 and 777 nm and (3) the water vapor content above and around convective clouds using the three shortwave infrared (SWIR) imagers, with a spatial resolution of 125 m at nadir.

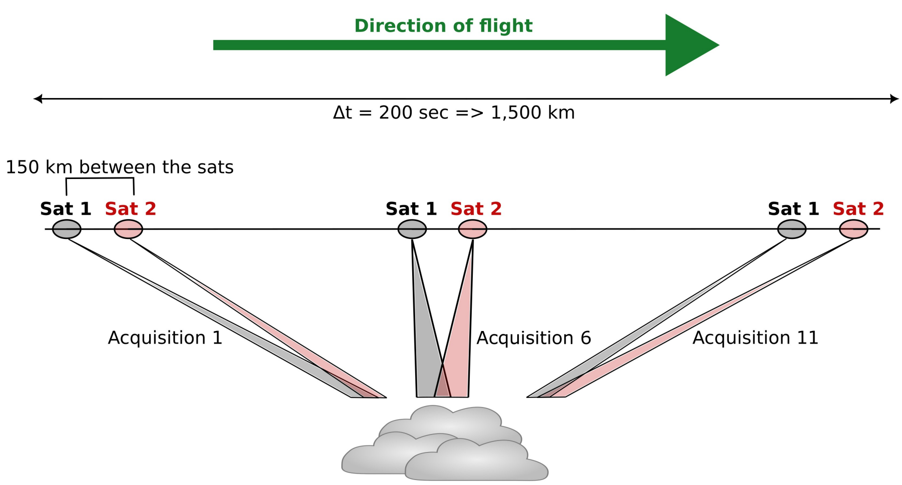

Figure 1. Illustration of the principle of the Cluster for Cloud evolution, ClImatE and Lightning (C^{3}IEL) observations.

This paper focuses on the development of a retrieval algorithm for the integrated water vapor content above cloud (IWV_{AC}) from three SWIR water vapor imagers on each satellite. Figure 2 shows the water vapor transmission spectrum in this spectral range and the three spectral bands selected for the C^{3}IEL water vapor imagers. The first band (1) is a non-absorbing band

https://doi.org/10.5194/egusphere-2025-787
Preprint. Discussion started: 6 March 2025

centered at 1.04 µm; the second band (2) is a moderately absorbing band centered at 1.13 µm; the third one is a highly absorbing band centered at 1.37 µm. These three bands have a spectral width of about 0.02 µm.

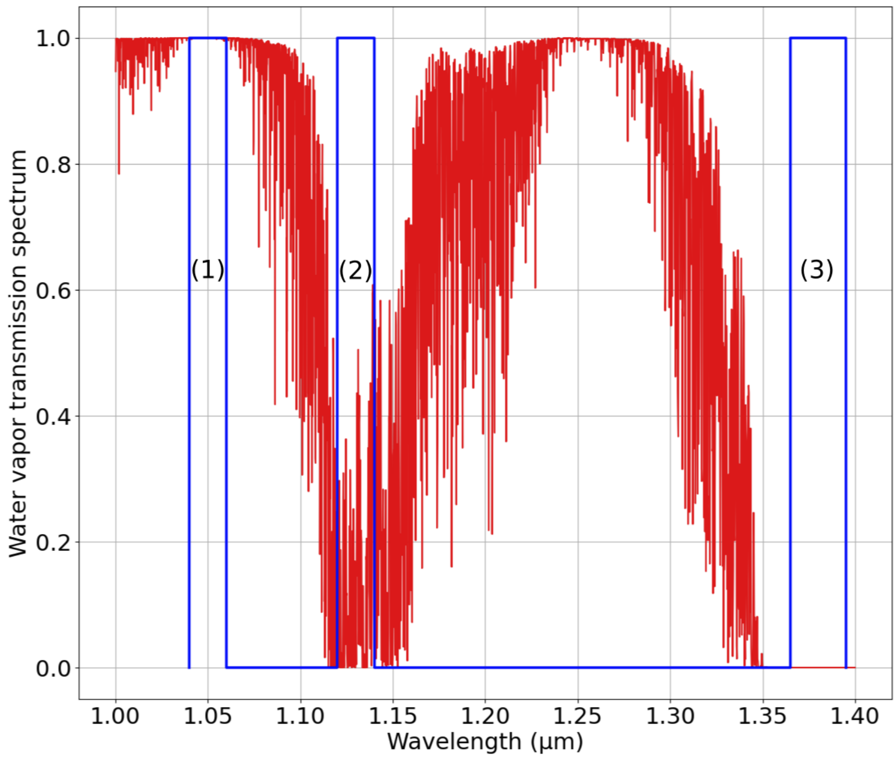

Figure 2. Water vapor transmission spectrum in clear sky condition at nadir (red curve) and the three SWIR spectral bands for the study of water vapor in the context of the C^{3}IEL space mission (blue rectangles).

3 Methodology

This section introduces the retrieval scheme used in our study. It follows an Optimal Estimation Method (OEM) scheme (Rodgers, 2000), with the aim to get the 1D equivalent cloud optical thickness (COT) and the integrated water vapor above cloud (IWV_{AC}). The OEM is a Bayesian statistical approach commonly used in remote sensing in order to estimate atmospheric and surface properties from measurements, such as satellite remote sensing (*e.g.,* Sourdeval et al., 2013, 2015; Leonarski et al., 2020; Matar et al., 2023). The objective of the OEM is to minimize the difference between the measured and the simulated radiances, under the constraint of *a priori* knowledge about the atmosphere. Equation (1) formalizes how the OEM works:

$$y = F(x,b) + \epsilon \quad (1)$$

https://doi.org/10.5194/egusphere-2025-787
Preprint. Discussion started: 6 March 2025

where the vector y contains the measured radiances and F denotes the forward model including the model assumed for the retrieval and the radiative transfer code to get radiances from atmospheric properties. The state vector (x) contains the parameters to retrieve (see section 3.1), whereas b specifies the fixed parameters within the forward model (see section 3.2). Lastly, the vector ϵ contains the errors assumed to be randomly distributed, encompassing measurement uncertainties, errors in the fixed parameters and related to the forward model. Because forward model errors are extremely hard to estimate properly, as usually done only uncertainties associated with measurements and fixed parameters are considered in this paper.

3.1 Measurement and state vectors: y and x

Water vapor retrieval in the context of the C^{3}IEL space mission is based on the exploitation of three spectral bands in the SWIR. The non-absorbing band (centered at 1.04 µm) is sensitive to the 1D equivalent cloud optical thickness (COT), representing the medium's reflectivity, while the two other bands (centered at 1.13 and 1.37 µm), which are also sensitive to the 1D equivalent COT, are used to retrieve the IWV_{AC}.

The measurement vector contains thus the radiance values measured in the three spectral bands described above:

$$y = \begin{bmatrix} R_{1.04} \\ R_{1.13} \\ R_{1.37} \end{bmatrix} \tag{2}$$

As the C^{3}IEL mission is still not in orbit, these radiances are simulated to develop and evaluate the algorithm using atmospheric and cloud profiles described in section 5. Measurement vector data are associated with an uncertainty of $5\ \%$.

The state vector contains the desired parameters, the 1D equivalent COT and IWV_{AC}:

$$x = \begin{bmatrix} \text{1D COT} \\ \text{IWV}_{AC} \end{bmatrix} \tag{3}$$

The uncertainty on the *a priori* knowledge is arbitrarily set to $10,000\ \%$, in order to minimize its influence and give more weight to the measurements during the retrieval process.

At the end of the OEM process, the variance-covariance matrix of the retrieved state vector is computed and gives the uncertainties on the retrieved parameters (*a posteriori* uncertainties, noted σ_x) with the following relationship (Rodgers, 2000):

$$\sigma_x = \sqrt{\left(S_a^{-1} + K_i^T S_\epsilon^{-1} K_i\right)^{-1}} \tag{4}$$

which is the square root of the *a posteriori* variance-covariance matrix. In this expression, S_a is the *a priori* variance-covariance matrix, K the jacobian, and S_ϵ the error variance-covariance matrix associated with the measurements and fixed parameters (see Appendix A for more details).

https://doi.org/10.5194/egusphere-2025-787
Preprint. Discussion started: 6 March 2025

3.2 Fixed parameters: b

The cloud model defined in the developed retrieval algorithm assumes a 1D horizontally and vertically homogeneous plane-parallel layer between the cloud base height (noted Z_b) and its top altitude (noted Z_t), horizontally infinite over the ocean. Table 1 describes the fixed parameters used in the developed retrieval algorithm and their uncertainties.

Table 1. Description of the fixed parameters and their uncertainties.

Fixed parameter (b)	Value	Uncertainty (ϵ_b)
Surface albedo	0.060	±0.006
cloud base height (Z_b)	0.71 km	± 0.32 km
cloud top height (Z_t)	provided by CLOUD/C^{3}IEL	± 0.04 km
Droplet [Ice] effective radius	10 [45] µm	± 5 µm

In this study, we consistently assign a surface albedo of 0.060, representing an ocean surface, with an uncertainty chosen to be 10 %. The cloud base height is set to 0.71 km with an uncertainty of 0.32 km. These values represent respectively the average and standard deviation values derived from the ECMWF-IFS selected profiles for this study (section 5.2.1). The cloud top height varies based on the atmospheric profile used to simulate the measurements. In practice, it will be determined by combining data from the pair of visible imagers designed for studying the 3D envelope and development velocities. The cloud top height uncertainty is set to 0.04 km (Dandini et al., 2022). For clouds with a top altitude above 4 km, we assume they consist of two distinct phases: a liquid phase between the cloud base height (Z_b) and $Z = 4$ km, and an ice phase between $Z = 4$ km and the cloud top height (Z_t). This fixed altitude of 4 km represents the average height of the 0 °C isotherm, according to the ECMWF profiles selected for this study. The effective radius of cloud droplets is fixed at an average value of 10 µm (*e.g.,* King et al., 2004), with an accuracy of 50 %. The effective radius of ice crystals is set to an average value of 45 µm with an associated uncertainty of 5 µm. These values represent the average and standard deviation of the ice effective radius calculated using the Wyser parameterization (Wyser, 1998) applied on the whole database described in section 5.2.1.

3.3 Radiative transfer model: F

Our study combined an Optimal Estimation Method with the radiative transfer code ARTDECO (Atmospheric Radiative Transfer Database for Earth and Climate Observation) in order to solve the Radiative Transfer Equation (RTE) by means of the adding-doubling model (de Haan et al., 1987). ARTDECO (https://www.icare.univ-lille.fr/artdeco/, Dubuisson et al., 2016) is a tool that gathers various models and data used to simulate Earth total and polarized atmosphere radiances and radiative fluxes, from the UV to the thermal IR range (200 nm to 50 µm). It uses the homogeneous plane-parallel approximation and allows to compute aerosols and clouds optical properties.

https://doi.org/10.5194/egusphere-2025-787
Preprint. Discussion started: 6 March 2025

3.4 IWV_{AC} retrieval: principle and assumptions

Given the limited information on the atmospheric profile from the measurements, assumptions are made to constrain the model: molecular Rayleigh scattering is disregarded due to its negligible effect in the SWIR, and relative humidity (RH) is assumed to be 100 % within the cloud.

As explained above, the main objective of the developed retrieval algorithm is to minimize the difference between the measured radiances and the radiances simulated by the forward model. The process begins with a first guess value for the state vector including the 1D equivalent cloud optical thickness (COT) and IWV_{AC}. In each iteration, the state vector is adjusted to achieve simulated radiances closer to the measured one. The COT, being an input parameter in the radiative transfer code, is subject to a direct adjustment at each iteration. The IWV_{AC} follows a different approach as it represents the vertical integration of the water vapor profile above clouds used in the forward model. The adjustment consists in applying, at each iteration, a multiplicative factor β to the water vapor profile, noted $h(z)$, from the cloud top height (Z_t) to the top of atmosphere. The resulting adjustment coefficient, β, is derived by calculating the ratio between the estimated IWV_{AC} at iteration $i+1$ and the one estimated at iteration i:

$$h_{i+1}(z) = \beta \cdot h_i(z) \quad (5)$$

with,

$$\beta = \frac{\mathcal{I}_{i+1}}{\mathcal{I}_i} \quad (6)$$

for clarity, we define $\mathcal{I} = IWV_{AC}$.

4 Sensitivity of water vapor spectral bands to IWV_{AC}

In this section, we examine how the radiances simulated in the water vapor spectral bands (1.13 and 1.37 µm) vary with IWV_{AC} (figure 3). Simulations are performed with atmospheric profiles derived from the Air Force Geophysics Laboratory (AFGL) database (Anderson et al., 1986).

To perform this sensitivity study we introduced a set of one hundred different clouds by combining ten different cloud top heights (Z_t) ranging from 1 to 10 km in order to have a large variability of IWV_{AC} (from 10^{-2} to 25 $\mathrm{kg.m^{-2}}$) and ten different cloud optical thicknesses (COT) ranging from 10 to 200. Figure 3(a) shows the results for these various cloud cases and exhibits, logically, a decrease in the simulated radiances as the IWV_{AC} increases. Indeed, the greater the apparent radiation path through the atmosphere is, the more water vapor the radiation interacts with. Consequently, water vapor absorption increases, leading to a decrease in radiance. Radiance sensitivity is particularly high at lower water vapor contents but decreases as the water vapor content increases.

Figure 3(b) shows that radiance in the 1.37 µm spectral band becomes negligible when water vapor content exceeds 5 $\mathrm{kg.m^{-2}}$. It does not reach zero in the 1.13 µm band for values until 25 $\mathrm{kg.m^{-2}}$. The 1.37 µm band is thus mainly useful in retrieving IWV_{AC} for low water content above cloud either in the presence of high-level clouds or in a dry atmosphere. It is

https://doi.org/10.5194/egusphere-2025-787
Preprint. Discussion started: 6 March 2025

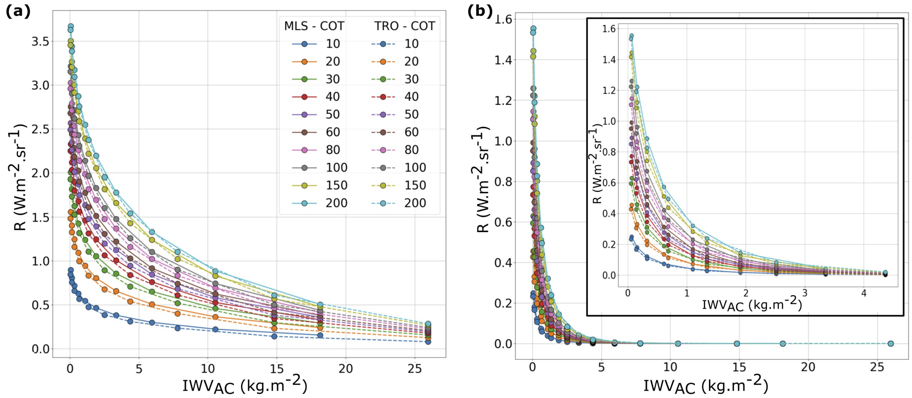

Figure 3. Simulated radiances of the C[3]IEL 1.13 µm band (a) and 1.37 µm band (b) as a function of IWV_{AC} for two atmospheric profiles from the AFGL database (Mid-Latitude Summer and Tropical profiles), for several cloud top heights (Z_t = 1, 2, 3, 4, 5, 6, 7, 8, 9, and 10 km), and various COT ranging from 10 to 200. In the figure (b), the rectangle represents a zoom of the figure for IWV_{AC} values between 0 and 5 $\mathrm{kg.m^{-2}}$. The Solar Zenith Angle (SZA) is set to 30 ° and the satellite observation angle (View Zenith Angle - VZA) is 0 ° (nadir).

also worth noting the non-overlapping color curves, where each color corresponds to a specific COT value. Despite the slight differences between them, this indicates a small sensitivity of these two spectral bands to the 1D equivalent COT.

5 IWV_{AC} retrieval

In a first hand, the retrieval algorithm presented in this paper is tested under idealized cloudy sky profiles using clear sky profiles from the AFGL database (Anderson et al., 1986), and then under realistic cloudy sky profiles, using atmospheric profiles provided by ECMWF-IFS database (https://www.nwpsaf.eu/site/software/atmospheric-profile-data/) to better evaluate its performance.

5.1 Using idealized cloudy profiles

This test set was built using the same approach as for the sensitivity test above, we artificially introduced a set of one hundred clouds in the AFGL database profiles, with a fixed cloud base height (Z_b) of 0.710 km and ten different cloud top heights ranging from 1 to 10 km. These artificial clouds are assumed to be composed entirely of water droplets with an effective radius of 10 µm and with a COT varying from 10 to 200. The solar incidence angle is set to 30 ° and the satellite observation angle is 0 ° (nadir). The target IWV_{AC} values are derived from the AFGL tropical profile, while the first guess profile used to start the retrieval process is the SAS (Sub-Arctic Summer) profile, due to its smooth gradient from the top to the bottom of the atmosphere. Tests conducted with different first guess profiles, both in idealized and realistic scenarios, give similar results. Therefore, the results presented in this paper are based on the use of the SAS profile as the first guess. In these idealized dataset

https://doi.org/10.5194/egusphere-2025-787
Preprint. Discussion started: 6 March 2025

tests, the cloud profile used to simulate the measurements is identical to the one used in the cloud inversion model for the retrieval (Section 3.2). The only difference arises from the water vapor profile.

As the relation between non-absorbing radiances and COT is well-known and widely used, figures related to the COT retrieval are not displayed here. Nevertheless, the developed retrieval algorithm allows to retrieve 1D equivalent COT with an average error less than 27.3 % for COT values below 100 (less than 20.5 % for values below 50). However, as it is well-known (*e.g.,* Nakajima and King, 1990; Nakajima et al., 1991), if the 1D equivalent COT exceed 100, an accurate retrieval becomes impossible because of the asymptotic behavior of the radiances as a function of cloud optical thickness for large COT values (an average error of around 47.3 % in this case).

The IWV_{AC} retrieval is tested for two measurement vectors: the first one with only the 1.04 and the 1.13 µm radiances and the other one with the three spectral bands centered at 1.04, 1.13 and 1.37 µm. Absolute errors (retrieved minus target values) are displayed in figure 4.

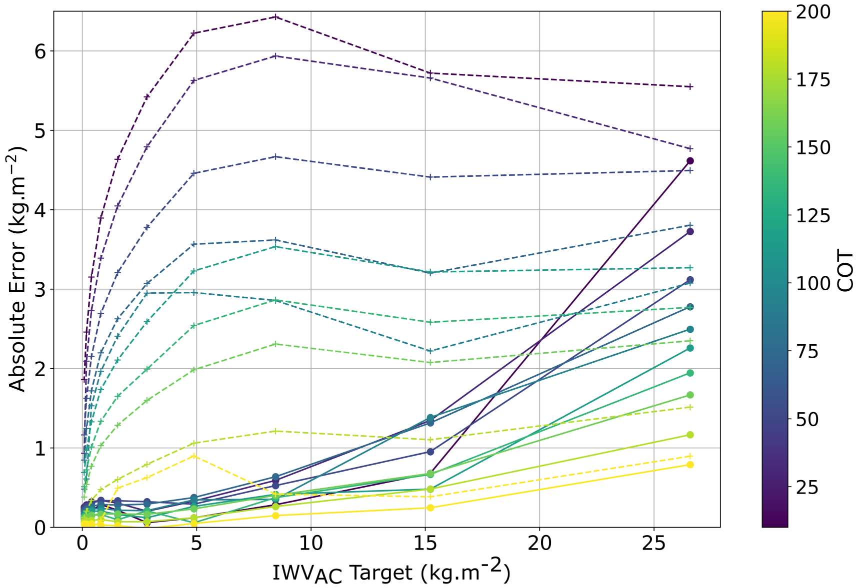

Figure 4. Absolute errors obtained for the IWV_{AC} retrieval (IWV_{AC} retrieved minus IWV_{AC} target) as a function of the IWV_{AC} target values. Dotted lines represent results obtained using only the 1.04 and 1.13 µm spectral bands, while full lines illustrate results using the three spectral bands (1.04, 1.13 and 1.37 µm) in the measurement vectors. The colorbar represents the different COT values.

Regardless of the measurement vector used (whether two or three radiances), an increase in the absolute error (IWV_{AC} retrieved minus IWV_{AC} target) is observed as the water vapor content increases and as the COT decreases. In other words, optically thin clouds exhibit a more pronounced absolute error due to the greater vertical penetration of radiation into the cloud leading to a better sensitivity to the water vapor profile inside the cloud. The absolute error is positive, indicating that the retrieved IWV_{AC} is overestimated. For each case, the assumed extinction profile used to generate the idealized radiance dataset

https://doi.org/10.5194/egusphere-2025-787
Preprint. Discussion started: 6 March 2025

is similar to the one defined in the model, the penetration of the radiation and multiple scattering effects are the same. The differences thus arise from the water vapor profile within the cloud. Indeed, during the retrieval process, the profile inside the cloud is not adjusted. The first guess profile (AFGL SAS profile) is drier than the target AFGL tropical profile. Consequently, less radiation is absorbed within the cloud with the SAS model used for the retrieval than with the AFGL tropical model used to simulate the test measurements. Consequently, to compensate for this lower absorption and minimize the difference between the forward model simulations $F(x)$ and the measurements y, the retrieved water vapor content above the cloud is overestimated.

When considering only the simulated radiances at 1.04 and 1.13 µm (dotted lines in figure 4), absolute errors increases rapidly for low IWV_{AC} values (below 5 kg.m^{-2}), to reach a peak above 6 kg.m^{-2} in the presence of optically thin clouds contrary to the retrieval with the three bands for which the absolute error remains less than 0.5 kg.m^{-2}. These results clearly shows that the highly absorbing band at 1.37 µm is essential to retrieve low water vapor content above clouds. Above 5 kg.m^{-2} the absolute errors values with two spectral bands remain roughly constant and get closer to the errors obtained using the three spectral bands as the 1.37 µm tends to be totally absorbed (radiances are close to 0).

When examining the combined information from the three spectral bands (solid lines), the absolute errors are significantly lower than 1 kg.m^{-2} for water vapor contents below 10 kg.m^{-2}, regardless of the optical thickness. As mentioned previously, as IWV_{AC} increases, the absolute errors also increase, particularly for thin clouds. In this case, we observe maximum absolute errors of about 3 to 5 kg.m^{-2} for cloud optical thickness (COT) values below 30. For optically thick clouds (COT > 80), the errors remains below 2 kg.m^{-2}, even for higher IWV_{AC} values. Overall, this figure highlights the necessity of using the three C^{3}IEL spectral bands to retrieve accurately the IWV_{AC}, and demonstrates good performance, especially for moderate to high optical thicknesses.

5.2 Using realistic cloudy profiles

The ECMWF-IFS database provides realistic atmospheric cloud profiles at 137 pressure levels, including profiles of temperature, specific humidity, cloud liquid and ice water, along with fractional cloud cover. It also provides surface data such as pressure, temperature and albedo.

5.2.1 Description of the realistic water vapor profiles

We use only profiles containing clouds located over the ocean, as the developed algorithm does not currently account for the surface below the clouds. Profiles at latitudes higher than 60 ° N/S are also excluded, since the C^{3}IEL mission will not observe at these latitudes. Additionally, the C^{3}IEL mission focuses on studying *cumulus congestus* and *cumulonimbus* clouds. Consequently, clear sky profiles and those containing only *cirrus* clouds have been discarded from our study. Finally, we choose to study single-layer clouds, excluding cases where a clear sky layer exists between two cloud layers. The same approach was applied for selecting high-level clouds, considering only continuous clouds with the condition that the cloud top height of the liquid phase ($Z_{t,liq}$) must be greater or equal to the cloud base height of the ice phase ($Z_{b,ice}$). Figure 5 shows the geographical distribution of the 232 selected profiles of low/mid level clouds and the 30 profiles corresponding to high-level clouds. For

https://doi.org/10.5194/egusphere-2025-787
Preprint. Discussion started: 6 March 2025

each profile, the IWV_{AC} is computed and is used as the target value, considered as the "truth". The distribution of these values are presented in figure 6.

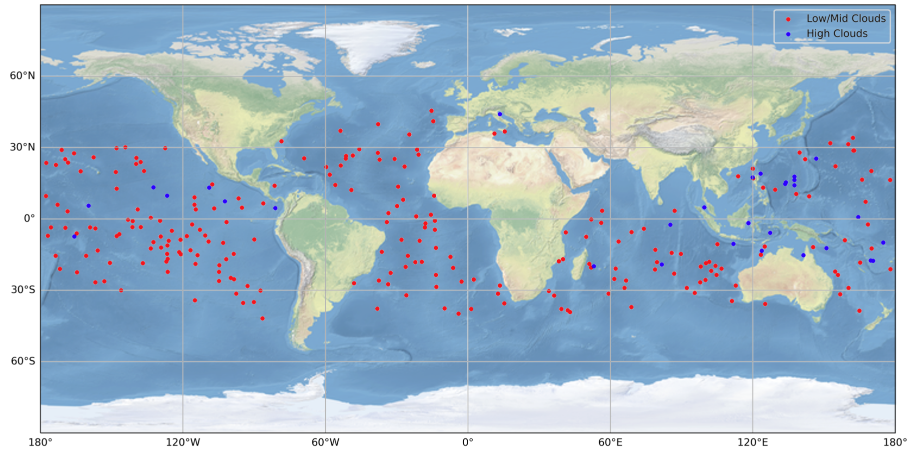

Figure 5. Geographical distribution of the selected profiles from the ECMWF-IFS database used to test the developed retrieval algorithm. A total of 262 profiles, including 232 profiles with low/mid-level clouds liquid-only clouds (red points), and 30 profiles with high-level mixed-phase clouds (blue points) are selected.

For the ECMWF-IFS profiles, the cloud base and cloud top height are obtained from the Liquid/Ice Water Content (respectively LWC and IWC) profiles. We look for the first and last values of the LWC and IWC profiles above a threshold of 10^{-3} $\mathrm{g.m^{-3}}$. The cloud phase is determined based on the LWC and IWC values, and the layers may be classified as liquid, ice or mixed phase. Then, in case of low/mid-level clouds, IWV_{AC} values range from 0.5 to $21.3\ \mathrm{kg.m^{-2}}$ but are predominantly below $15\ \mathrm{kg.m^{-2}}$. Regarding high-level clouds, the values range from approximately $0.06\ \mathrm{kg.m^{-2}}$ to $0.9\ \mathrm{kg.m^{-2}}$. Initially, the database did not include enough clouds at mid-high altitudes ($6-10$ km). To compensate for this deficiency, the cloud top height is artificially decreased by 4 km. As a result, the IWV_{AC} calculations for high-level clouds are derived from these adjusted profiles.

5.2.2 Results of the IWV_{AC} retrieval: Low-/Mid-level clouds

Simulations are performed using three different Solar Zenith Angles ($SZA = 0$ °, 30 °, and 60 °) and 11 Viewing Zenith Angles (VZA), based on the C^{3}IEL planned acquisition sequence, resulting in a total of $7,656$ retrievals. As for retrievals under idealized conditions, the first guess profile is the SAS profile and the figures and analyses focus only on the IWV_{AC} retrieval. However, the algorithm developed also allows for the retrieval of the 1D equivalent cloud optical thickness (COT) and shows an average absolute error of -2 for $COT < 100$. In contrast, for $COT > 100$, the COT retrieval exhibits larger errors due to the asymptotic behavior of radiance as a function of COT. Figure 7 illustrates the relationship between the retrieved and target values of the IWV_{AC} along the radiation path in the atmosphere (noted $mIWV_{AC}$), where $mIWV_{AC}$ is calculated as the IWV_{AC} multiplied by the air mass factor m, defined as:

https://doi.org/10.5194/egusphere-2025-787
Preprint. Discussion started: 6 March 2025

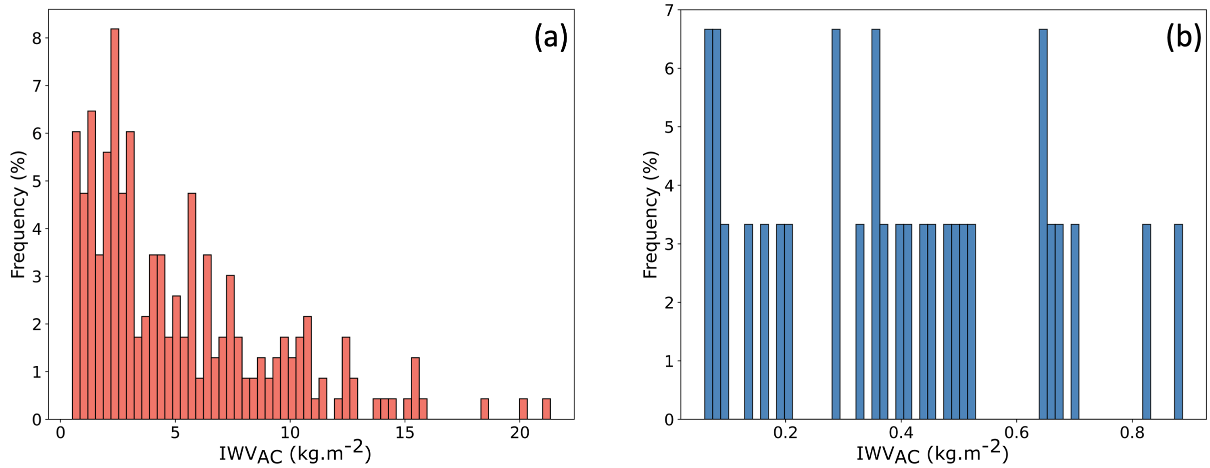

Figure 6. Distribution of IWV_{AC} values calculated from the selected profiles. (a) target IWV_{AC} values for the 232 profiles containing low/mid-level clouds, (b) target values for the 30 profiles containing high-level clouds.

$$m = \frac{1}{\cos(SZA)} + \frac{1}{\cos(VZA)} \quad (7)$$

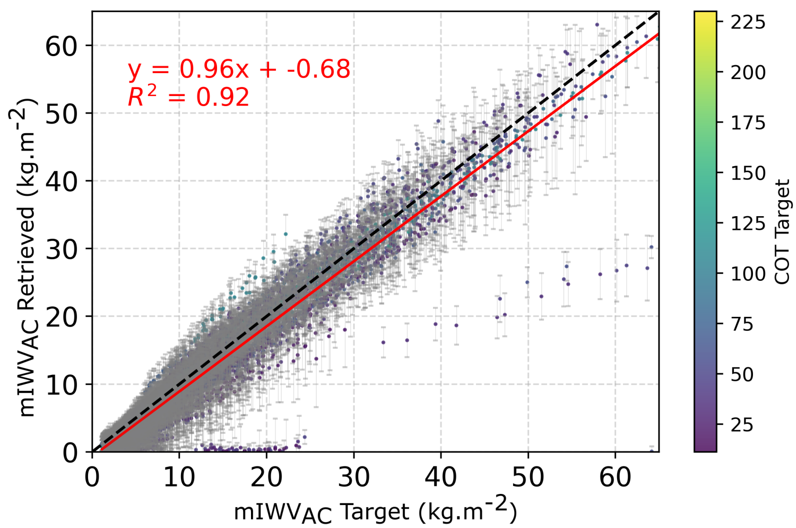

Figure 7. Relationship between the retrieved and target $mIWV_{AC}$ values for profiles containing low-/mid-level clouds. The red line represents the linear regression and the black dashed line indicates the $y = x$ line. Error bars represent the uncertainty estimated by the retrieval algorithm.

https://doi.org/10.5194/egusphere-2025-787
Preprint. Discussion started: 6 March 2025

A good correlation is observed between the retrieved and target values, as indicated by a score (R^2) of 0.92 and the linear regression equation as a slope of 0.96 with a small systematic under-estimation of -0.68 kg.m^{-2}. A convergence rate of 94 % was achieved, indicating that 94 % of the profiles and geometries successfully converge to a value above the threshold limit of 0.01 kg.m^{-2}. The 6 % of profiles that do not converge correspond to low and optically thin clouds, primarily clouds below 2 km and with a COT below 20, which is consistent with results obtained for idealized cases. The non convergence cases and the largest errors comes from the cloud base height (Z_b) errors and the way of computing to cloud extinction profile (C_{ext}), assumed to be vertically homogeneous and defined as the ratio of cloud optical thickness (COT) to its geometric thickness (Z_t-Z_b). In this study, the cloud base height is defined as the average value of the ECMWF-IFS Z_b distribution, associated with an uncertainty of 45 %, which represents, for low-level clouds, a large geometrical thickness uncertainty, impacting the cloud extinction coefficient value and the cloud vertical penetration. These results corroborate the conclusions of Albert et al. (2001) and the results obtained in section 5.1.

The error bars in Figure 7 represent the *a posteriori* uncertainty estimated by the retrieval algorithm. These errors comes from the errors measurement and the fixed (or non-retrieved) parameters. Although the results from the algorithm are satisfactory, only 71 % of the retrievals and their associated errors capture the target value within the 3-sigma confidence interval. It highlights the limitation of the current developed algorithm to accurately take into account the errors, *e.g.* coming from the forward model $F(x)$. Since no information is available regarding the "true" extinction profiles in the measurements, the typical assumption of vertical uniformity is employed, and errors related to this assumption are not included in the error variance-covariance matrix. Furthermore, after additional analysis, it was found that the unsatisfactory uncertainties correspond again to low-level clouds (Z_t < 2.5 km) and/or thin clouds ($COT < 30$). Regarding the statistics for the entire dataset, the absolute error distribution is shown in Figure 8(a). Results show an average value of -0.46 kg.m^{-2} and a standard deviation of 1.2 kg.m^{-2}, indicating a small underestimation of the retrieved IWV_{AC} in average. To further refine and better characterize the retrieval algorithm's behavior, RMSE values have been calculated according to cloud optical thickness (COT) and cloud top height (Z_t) ranges as shown in Figure 8(b).

As already seen for idealized cases, the RMSE values for IWV_{AC} are clearly higher for low-level and thin clouds, with values generally exceeding 1.5 kg.m^{-2}. The RMSE decreases as Z_t and COT increase. RMSE values are below 0.8 kg.m^{-2} for $Z_t > 2{,}000$ m and $COT > 50$ and reach around 0.3 kg.m^{-2} for $Z_t > 3{,}000$ m and $COT > 120$. In optically thicker clouds, the penetration of radiation into the cloud-top layers is reduced, minimizing the impact of the extinction and water vapor profile assumptions used in the forward model. Additionally, as the cloud altitude increases from low to mid-level, the IWV_{AC} decreases rapidly, enhancing the sensitivity of the 1.37 µm band, as demonstrated in the idealized cases (Figure 4).

5.2.3 Results of the IWV_{AC} retrieval: High-level clouds

As for low-/mid-level clouds, retrievals have been calculated for the same 33 geometries, which lead to a total of 990 retrievals. Results for $mIWV_{AC}$ are presented in Figure 9. In comparison with Figure 7, the convergence rate for high-level clouds is now 100 %. This is due to the absence of low-level or optically thin clouds in the selected profiles. For this type of clouds, COT values exceed 100 allowing the retrieval algorithm to converge for every profile. In terms of COT retrieval, the errors become

https://doi.org/10.5194/egusphere-2025-787
Preprint. Discussion started: 6 March 2025

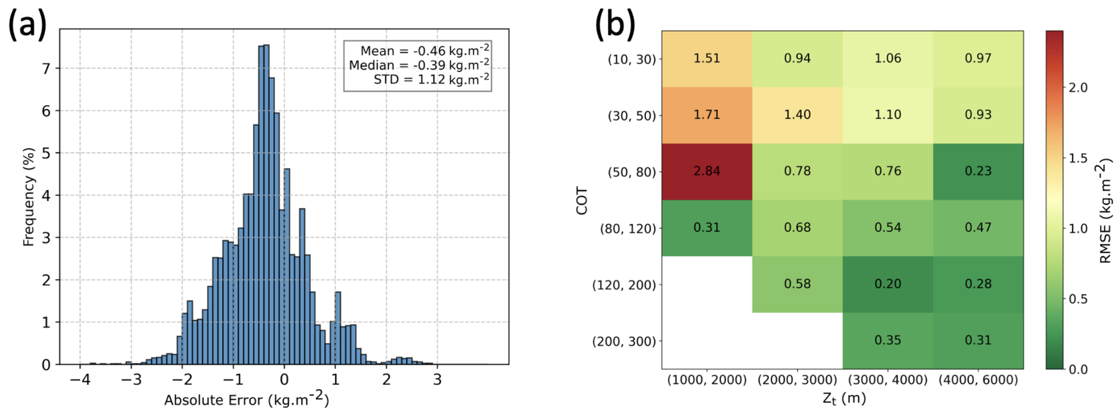

Figure 8. a) Distribution of the absolute error (retrieved minus target) for the whole dataset, and b) RMSEs calculated according to various Z_t, and COT ranges.

considerable as beyond an optical thickness of 100, the spectral band sensitivity at 1.04 µm is not sufficient to have a reliable retrieval under the assumption of an infinite cloud. The extinction profile in the cloud model used for the retrieval is thus impacted accordingly. Regarding the $mIWV_{AC}$ retrieval, the algorithm tends to overestimate the $mIWV_{AC}$ retrieved value for most of the cases with a linear regression slope of 1.60 and a relatively important dispersion as the R^2 score is 0.52. These less favorable results, compared to the low- and mid-level cloud cases, are primarily due to six profiles (198 retrievals) where large discrepancies exist between the observed extinction profiles and those assumed in the retrieval algorithm, as discussed in the following section. Overall 76 % of the retrieved $mIWV_{AC}$ values and their uncertainties capture the target values for high-levels clouds (within the 3-sigma confidence interval), with a global IWV_{AC} RMSE of 0.56 $\mathrm{kg.m^{-2}}$.

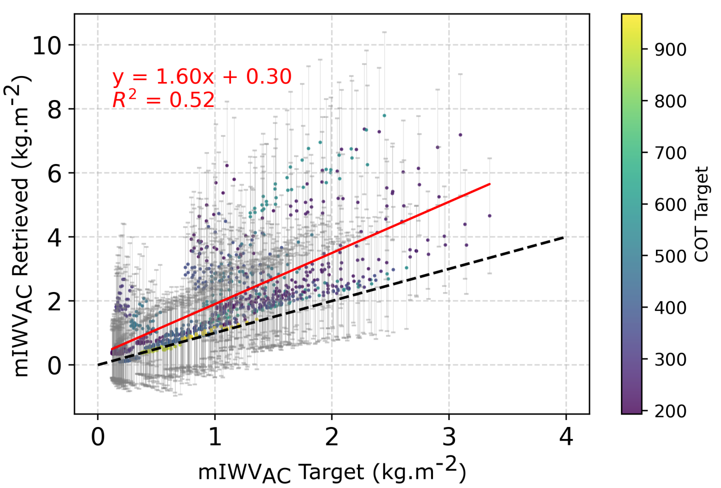

Figure 9. Same as Figure 7 but for profiles containing high-level clouds.

https://doi.org/10.5194/egusphere-2025-787
Preprint. Discussion started: 6 March 2025

5.2.4 Discussion concerning the underestimation or overestimation of the retrieved IWV_{AC}

As stated in the Figure 9 comments, there is a quasi systematic overestimation of the retrieved IWV_{AC} value for the mixed-phase clouds while there is a small underestimation in the case of liquid clouds (Figure 8(a)).

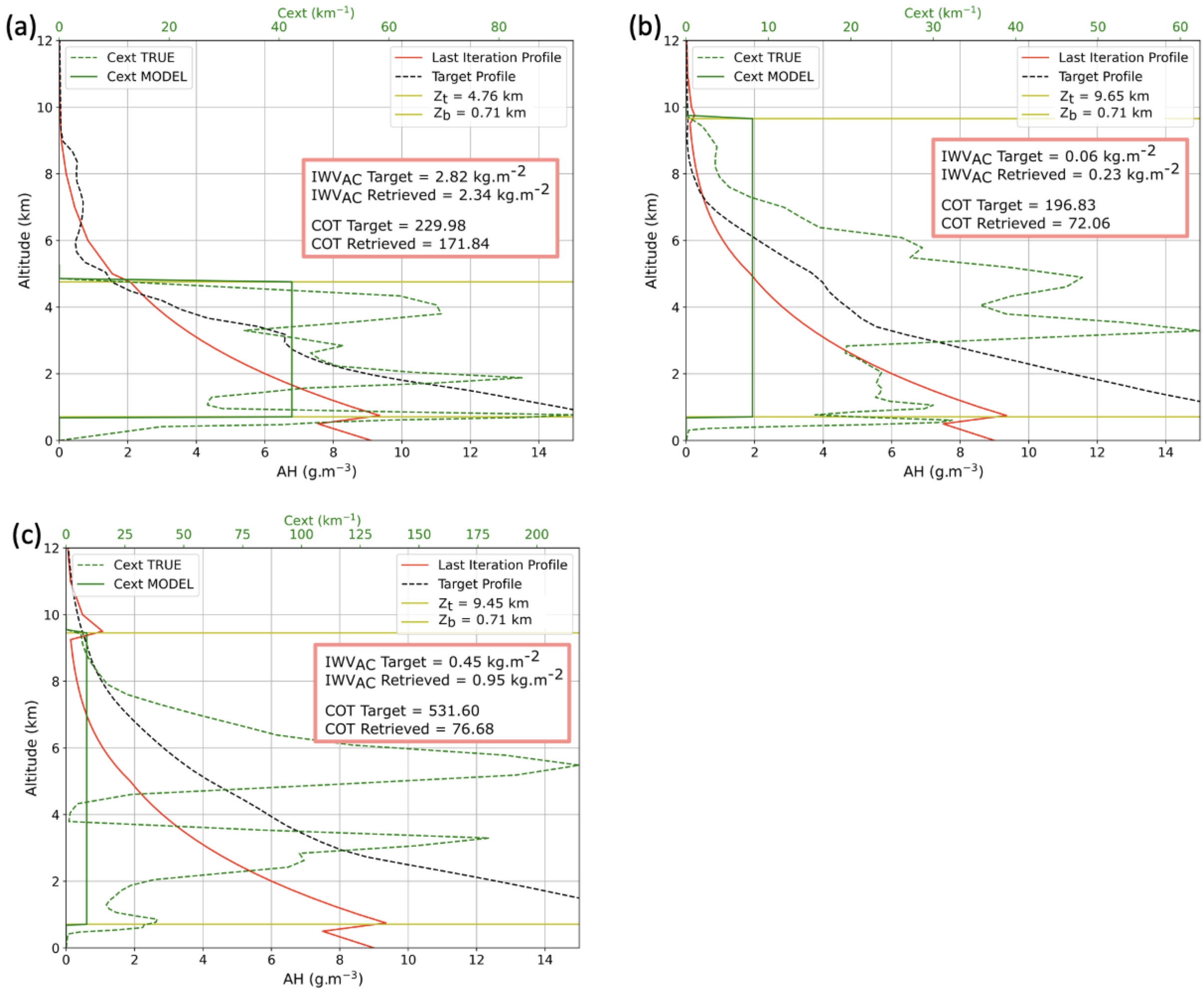

Figure 10. Absolute humidity and extinction profiles derived from the ECMWF-IFS database and retrieved from the developed retrieval algorithm. Three cases are showed to illustrate the underestimation of IWV_{AC} for liquid cloud cases in (a), the overestimation of IWV_{AC} for the mixed-phase clouds in (b) and (c). The dashed black line indicates the "true" water vapor profile and the solid red line, the water vapor profile obtained at the last iteration of the OEM. The dashed green curve represents the "true" cloud extinction profile while the solid green line corresponds to the cloud model extinction profile. Z_b and Z_t are represented by horizontal yellow lines.

We identified three cases that explain the underestimation, Figure 10(a), or overestimation, Figure 10(b) and Figure 10(c), of the water vapor content above the clouds. In this figure, realistic absolute humidity (black dashed lines) and extinction profiles

https://doi.org/10.5194/egusphere-2025-787
Preprint. Discussion started: 6 March 2025

(green dashed line) within the cloud (obtained from the ECMWF-IFS database) are plotted alongside profiles retrieved with the forward model assumptions. The dark green lines represent vertically uniform cloud extinction profiles, while the solid red lines depict water vapor profiles, assuming $100\ \%$ relative humidity within the cloud for the SAS profile. The cloud top height (Z_t) and cloud base height (Z_b) are delimited by yellow horizontal lines.

In Figure 10(a), the extinction coefficient in the upper cloud layers is lower in the model compared to the "true" extinction profile. This leads to deeper vertical penetration of radiation into the cloud compared to the realistic profile, resulting to increase the absorption by water vapor within the cloud. To compensate for this effect, the retrieval algorithm reduces absorption above the cloud resulting in lower IWV_{AC} (2.34 vs 2.82 $\mathrm{kg.m^{-2}}$) in order to minimize the difference between the measured (y in Eq. (1)) and simulated radiances $F(x,b)$.

In Figure 10(b), although the algorithm tends to underestimate the total COT, it overestimates the extinction profile in the upper layers (above $7\ \mathrm{km}$). This overestimation reduces the cloud penetration and, consequently, the in-cloud absorption. To compensate this effect the algorithm overestimates the IWV_{AC} (0.23 vs 0.06 $\mathrm{kg.m^{-2}}$). Additionally, the in-cloud water vapor profile (dashed black line) is higher in the realistic profile. When combined with the greater radiation penetration, this amplifies the absorption difference between the target and the retrieved value, further contributing to the overestimation.

Figure 10(c) shows a second example that leads to an overestimation of the retrieved IWV_{AC}. In this case, the algorithm underestimates the retrieved COT but the extinction profile within the upper part of the cloud is very similar to the observed one, which means that cloud penetration between the observation and the retrieval is consistent. The main difference lies in the in-cloud humidity profile which is largely underestimated in the model, leading to less in-cloud absorption and thus an overestimation of the IWV_{AC}.

The combined effects of under/overestimation of the top layers extinction coefficient and the under/overestimation of the in-cloud humidity are certainly the main source of errors in the current algorithm. Note that these effects can sometimes counterbalance each other, for example in case of less vertical penetration into the cloud associated to higher absolute humidity values.

6 Conclusions

The objective of this study is to show the feasibility of estimating the integrated water vapor content above cloud (IWV_{AC}) and the cloud optical thickness (COT), in the context of a future space mission project named C^{3}IEL (Cluster for Cloud evolution, ClImatE, and Lightning) in order to develop a retrieval algorithm. This mission aims at investigating the development of convective clouds with a high spatial and temporal resolution, the electrical activity associated with these clouds, and the water vapor content above and around cloud. The developed algorithm is based on a Bayesian probabilistic approach, the Optimal Estimation Method (OEM), which is an iterative fitting method. It is similar to the least square method but it offers additional possibilities as it permits to consider not only the measurement itself but also supplementary information (fixed parameters, *a priori* knowledge, *etc.*) as well as associated uncertainties for the estimation of several variables.

https://doi.org/10.5194/egusphere-2025-787
Preprint. Discussion started: 6 March 2025

A study has been conducted to evaluate if the three SWIR spectral bands of the C^{3}IEL mission can be used to retrieve the integrated water vapor content above cloud (IWV_{AC}). First, using simulations in the two water vapor spectral bands (1.13 and 1.37 µm), we show that radiance values decreases as IWV_{AC} increases because of the water vapor absorption. We note that the simulated radiances in the highly absorbing band (1.37 µm) tends toward 0 for IWV_{AC} values greater than $5\ \mathrm{kg.m^{-2}}$, *i.e.,* emphasizing the fact that this band is mainly useful for low IWV_{AC}, in dry atmosphere or above high clouds.

The developed algorithm is then first tested under idealized cloudy sky conditions with homogeneous cloud extinction profiles as assumed in the inversion model. The absolute errors of IWV_{AC} tends to increase as IWV_{AC} increases and COT decreases, thus the vertical penetration in the cloud. We also demonstrate the advantages of combining the two water vapor spectral bands, specifically, for the low water vapor content values where the absolute errors when combining the two spectral bands remains below $0.5\ \mathrm{kg.m^{-2}}$, regardless of the cloud optical thickness.

Then, the algorithm was tested on realistic profiles obtained from the ECMWF-IFS database. We focused on profiles featuring exclusively cloudy sky conditions over the ocean and within a latitude range of 60 ° N/S. We identified 232 cloudy profiles containing low-/mid-level clouds and 30 profiles containing high-level clouds (excluding cirrus). The algorithm exhibited a 94 $\%$ convergence rate for realistic profiles with low-/mid-level clouds. The IWV_{AC} results show a good correlation between the retrieved values and the target values (R^2 of 0.92 and a slope of 0.96). The RMSE is below $1\ \mathrm{kg.m^{-2}}$ for COT values above 50. The RMSE tends to increase for low clouds and low cloud optical thickness. In case of high clouds, the IWV_{AC} values are low so more difficult to retrieve. The RMSE is however still less than $1\ \mathrm{kg.m^{-2}}$. The linear regression slope is 1.60 and the score is 0.52. The analysis shows that the errors comes mainly from the extinction profiles and water vapor profiles assumed in the inversion model.

The algorithm presented in this paper is a preliminary one and could be improved. A way can be to use a more typical and realistic cloud extinction profiles in both liquid and mixed-phase clouds. This non-uniform profile can use a simple parametrization (*e.g.,* Matar et al., 2023) or be based on radar measurements (*e.g.,* Carbajal Henken et al., 2014). This improvement could possibly reduce the bias. Another way relies on the fixed parameters accuracy of cloud base height and effective radius, which both significantly affect cloud extinction values and difference in cloud vertical penetration. To improve the determination of these values, climatological data of Z_b or R_e, specific to the geographical location of the measurements could be used. In the same way, temperature profile climatology could be used to better constrain the $RH = 100\%$ assumption in the cloud model. Furthermore, research works have to be done to exploit the multi-views of the C^{3}IEL mission. The use of two simultaneous view angles should help reduce the uncertainties by better constraining the retrieval. However, using acquisitions spaced 20 s apart requires the development of a more complex algorithm, as the retrieved cloud top height will vary between two successive acquisitions. Moreover, at the observation scale of approximately 125 m, 3D radiative transfer can introduce effects such as radiative smoothing (*e.g.,* Marshak, 1995; Davis et al., 1997), as well as illumination and shadowing Várnai (2000) that roughen the radiative fields. These factors influence shortwave radiances and may impact the retrieval of water vapor content above clouds even if 3D radiative effects are anticipated to impact both absorbing and non-absorbing bands similarly due to their close spectral proximity. However, in addition for tilted view geometry of a finite cloud, the cloud base may appears significantly higher in the atmosphere than assumed in the cloud model, which could impact retrieval accuracy. To assess the

https://doi.org/10.5194/egusphere-2025-787
Preprint. Discussion started: 6 March 2025

assumption of a flat, homogeneous, and infinite cloud, more realistic cloud representations using 3D radiative simulations would be required to compute the measurements. This is a significant task beyond the scope of this paper, which aims to explore, as a first step, the possibility of retrieving integrated water vapor above clouds.

Appendix A: Variables from the *a posteriori* variance-covariance matrix

In our study, the *a priori* variance-covariance matrix (see Eq. (4)) is a diagonal matrix where the diagonal terms are the squared standard deviations for each parameter contained in the *a priori* state vector:

$$S_a = \begin{bmatrix} \sigma^2_{COT} & 0 \\ 0 & \sigma^2_{IWV_{AC}} \end{bmatrix} \tag{A1}$$

with σ_{COT} and $\sigma_{IWV_{AC}}$ obtained by multiplying the *a priori* state vector x_a by the arbitrarily chosen *a priori* error.

S_ϵ, the error variance-covariance matrix is expressed, in our study, as follows:

$$S_\epsilon = S_y + S_{fp} \tag{A2}$$

S_y is the measurement variance-covariance matrix, and S_{fp} describes the variance-covariance matrix linked to the fixed parameters:

$$S_y = \begin{bmatrix} \sigma^2_{y1} & 0 & 0 \\ 0 & \sigma^2_{y2} & 0 \\ 0 & 0 & \sigma^2_{y3} \end{bmatrix} \tag{A3}$$

and,

$$S_{fp} = K_b S_b K_b^T \tag{A4}$$

with,

$$K_b = \left.\frac{dF(b)}{db}\right|_x = \left.\frac{F(b+db) - F(b)}{db}\right|_x \tag{A5}$$

where b represent the fixed parameter (see table 1) and db is equal to $1\ \%$ of the fixed parameter value. S_b is a diagonal matrix whose diagonal elements represent the squared standard deviation associated with the different fixed parameters of the forward model:

$$S_b = \begin{bmatrix} \sigma^2_{Albedo} & 0 & 0 & 0 & 0 \\ 0 & \sigma^2_{Z_b} & 0 & 0 & 0 \\ 0 & 0 & \sigma^2_{Z_t} & 0 & 0 \\ 0 & 0 & 0 & \sigma^2_{R_{e,droplet}} & 0 \\ 0 & 0 & 0 & 0 & \sigma^2_{R_{e,ice}} \end{bmatrix} \tag{A6}$$

The different elements of this matrix are obtained by calculating the product of the relevant fixed parameter with the uncertainty attributed to it (see table 1).

https://doi.org/10.5194/egusphere-2025-787
Preprint. Discussion started: 6 March 2025

Author contributions. Each author has played a significant role in the development and scientific exploration presented in this study. RP and GP performed the study, developed the algorithm and write the original draft of the article. CC provided support for radiative transfer simulations and the analysis of corresponding data and retrieval results. OP contributed to the analysis of the atmospheric database (ECMWF-IFS) and the interpretation of retrieval results as well. CP offered expertise in the optimal estimation method and contributed to the analysis of radiative transfer simulations and retrieval outcomes.

Competing interests. There is no competing interests.

Acknowledgements. We are grateful to the CNES/TOSCA program which has funded this work as part of the preparation of the Cluster for Cloud evolution, Climate and Lightning French-Israeli space mission project. We acknowledge the AERIS/ICARE data center for providing the ARTDECO radiative transfer code free of charge. We would also like to thank L-C. Labonnote for his precious help and expertise on the ARTDECO tool and F. Thieuleux for his precious help during the development of the retrieval algorithm.

https://doi.org/10.5194/egusphere-2025-787
Preprint. Discussion started: 6 March 2025

References

Albert, P., Bennartz, R., and Fischer, J.: Remote Sensing of Atmospheric Water Vapor from Backscattered Sunlight in Cloudy Atmospheres, Journal of Atmospheric and Oceanic Technology, https://doi.org/10.1175/1520-0426(2001)018<0865:RSOAWV>2.0.CO;2, 2001.

Anderson, G. P., Chetwynd, J. H., and She, E. P.: AFGL Atmospheric Constituent Profiles (0-120km), p. 47, 1986.

Bennartz, R. and Fischer, J.: Retrieval of columnar water vapour over land from backscattered solar radiation using the Medium Resolution Imaging Spectrometer, Remote Sensing of Environment, pp. 274–283, https://doi.org/10.1016/S0034-4257(01)00218-8, 2001.

Blyth, A. M.: Entrainment in Cumulus Clouds, American Meteorological Society, https://doi.org/10.1175/1520-0450(1993)032<0626:eicc>2.0.co;2, 1993.

Bony, S., Stevens, B., Frierson, D. M. W., Jakob, C., Kageyama, M., Pincus, R., Shepherd, T. G., Sherwood, S. C., Siebesma, A. P., Sobel, A. H., Watanabe, M., and Webb, M. J.: Clouds, circulation and climate sensitivity, Nature Geoscience, pp. 261–268, 2015.

Bouffiès, S., Bréon, F. M., Tanré, D., and Dubuisson, P.: Atmospheric water vapor estimate by a differential absorption technique with the polarisation and directionality of the Earth reflectances (POLDER) instrument, Journal of Geophysical Research: Atmospheres, pp. 3831–3841, https://doi.org/10.1029/96JD03126, 1997.

Carbajal Henken, C. K., Lindstrot, R., Preusker, R., and Fischer, J.: FAME-C: cloud property retrieval using synergistic AATSR and MERIS observations, https://doi.org/10.5194/amtd-7-4909-2014, 2014.

Crutzen, P. J. and Ramanathan, V.: The Parasol Effect on Climate, Science, pp. 1679–1681, https://doi.org/10.1126/science.302.5651.1679, 2003.

Dandini, P., Cornet, C., Binet, R., Fenouil, L., Holodovsky, V., Y. Schechner, Y., Ricard, D., and Rosenfeld, D.: 3D cloud envelope and cloud development velocity from simulated CLOUD (C3IEL) stereo images, Atmospheric Measurement Techniques, pp. 6221–6242, https://doi.org/10.5194/amt-15-6221-2022, 2022.

Davis, A., Marshak, A., Cahalan, R., and Wiscombe, W.: The Landsat Scale Break in Stratocumulus as a Three-Dimensional Radiative Transfer Effect: Implications for Cloud Remote Sensing, Journal of the Atmospheric Sciences, pp. 241–260, https://doi.org/10.1175/1520-0469(1997)054<0241:TLSBIS>2.0.CO;2, 1997.

de Haan, J. F., Bosma, P. B., and Hovenier, J. W.: The adding method for multiple scattering calculations of polarized light, Astronomy and Astrophysics, 1987.

Desbois, M., Capderou, M., Eymard, L., Roca, R., Viltard, N., Viollier, M., and Karouche, N.: Megha-Tropiques : un satellite hydrométéorologique franco-indien, La Météorologie, https://doi.org/10.4267/2042/18185, 2007.

Dubuisson, P., C.-Labonnote, L., Riedi, J., Compiègne, M., and Winiarek, V.: ARTDECO : Atmospheric Radiative Transfer Database for Earth and Climate Observation, in: International Radiation Symposium, Auckland, New Zealand, 2016.

Fermepin, S. and Bony, S.: Influence of low-cloud radiative effects on tropical circulation and precipitation, Journal of Advances in Modeling Earth Systems, pp. 513–526, https://doi.org/10.1002/2013MS000288, 2014.

Gao, B. C. and Kaufman, Y. J.: Water vapor retrievals using Moderate Resolution Imaging Spectroradiometer (MODIS) near-infrared channels, Journal of Geophysical Research: Atmospheres, https://doi.org/10.1029/2002jd003023, 2003.

Harrison, E. F., Minnis, P., Barkstrom, B. R., Ramanathan, V., Cess, R. D., and Gibson, G. G.: Seasonal variation of cloud radiative forcing derived from the Earth Radiation Budget Experiment, Journal of Geophysical Research: Atmospheres, https://doi.org/10.1029/JD095iD11p18687, 1990.

https://doi.org/10.5194/egusphere-2025-787
Preprint. Discussion started: 6 March 2025

Hilton, F., Armante, R., August, T., Barnet, C., Bouchard, A., Camy-Peyret, C., Capelle, V., Lieven, C., Clerbaux, C., Coheur, P.-F., Collard, A., Crevoisier, C., Dufour, G., Edwards, D., Faijan, F., Fourrié, N., Gambacorta, A., Goldberg, M., Guidard, V., Hurtmans, D., Illingworth, S., Jacquinet-Husson, N., Kerzenmacher, T., Klaes, D., Lavanant, L., Masiello, G., Matricardi, M., McNally, A., Newman, S., Pavelin, E., Payan, S., Péquignot, E., Peyridieu, S., Phulpin, T., Remedios, J., Schlüssel, P., Serio, C., Strow, L., Stubenrauch, C., Taylor, J., Tobin, D., Wolf, W., and Zhou, D.: Hyperspectral Earth Observation from IASI: Five Years of Accomplishments, Bulletin of the American Meteorological Society, https://doi.org/10.1175/BAMS-D-11-00027.1, 2012.

Jensen, E. J., Toon, O. B., Selkirk, H. B., Spinhirne, J. D., and Schoeberl, M. R.: On the formation and persistence of subvisible cirrus clouds near the tropical tropopause, Journal of Geophysical Research: Atmospheres, https://doi.org/10.1029/95JD03575, 1996.

Karbou, F., Aires, F., Prigent, C., and Eymard, L.: Potential of Advanced Microwave Sounding Unit-A (AMSU-A) and AMSU-B measurements for atmospheric temperature and humidity profiling over land, Journal of Geophysical Research: Atmospheres, https://doi.org/10.1029/2004JD005318, 2005.

King, M. D., Platnick, S., Yang, P., Arnold, G. T., Gray, M. A., Riedi, J. C., Ackerman, S. A., and Liou, K.-N.: Remote Sensing of Liquid Water and Ice Cloud Optical Thickness and Effective Radius in the Arctic: Application of Airborne Multispectral MAS Data, Journal of Atmospheric and Oceanic Technology, pp. 857–875, https://doi.org/10.1175/1520-0426(2004)021<0857:RSOLWA>2.0.CO;2, 2004.

Lee, J., Yang, P., Dessler, A. E., Gao, B.-C., and Platnick, S.: Distribution and Radiative Forcing of Tropical Thin Cirrus Clouds, Journal of the Atmospheric Sciences, https://doi.org/10.1175/2009JAS3183.1, 2009.

Leonarski, L., C.-Labonnote, L., Compiègne, M., Vidot, J., Baran, A. J., and Dubuisson, P.: Potential of Hyperspectral Thermal Infrared Spaceborne Measurements to Retrieve Ice Cloud Physical Properties: Case Study of IASI and IASI-NG, Remote Sensing, https://doi.org/10.3390/rs13010116, 2020.

Lynch, D. K., ed.: Cirrus, Oxford University Press, Cambridge ; New York, ISBN 9780195130720, 2002.

Marshak, A.: The verisimilitude of the independent pixel approximation used in cloud remote sensing, Remote Sensing of Environment, pp. 71–78, https://doi.org/10.1016/0034-4257(95)00016-T, 1995.

Masson-Delmotte, V. P., Zhai, A., Pirani, S. L., Connors, C., Péan, S., Berger, N., Caud, Y., Chen, L., Goldfarb, M. I., Gomis, M., Huang, K., Leitzell, E., Lonnoy, J. B. R., Matthews, T. K., Maycock, T., Waterfield, O., Yelekçi, R. Y., and Zhou, B.: Climate Change 2021: The Physical Science Basis. Contribution of Working Group I to the Sixth Assessment Report of the Intergovernmental Panel on Climate Change, Cambridge University Press. In Press., 2021.

Matar, C., Cornet, C., Parol, F., C.-Labonnote, L., Auriol, F., and Nicolas, M.: Liquid cloud optical property retrieval and associated uncertainties using multi-angular and bispectral measurements of the airborne radiometer OSIRIS, Atmospheric Measurement Techniques, https://doi.org/10.5194/amt-16-3221-2023, 2023.

McFarquhar, G. M., Heymsfield, A. J., Spinhirne, J., and Hart, B.: Thin and Subvisual Tropopause Tropical Cirrus: Observations and Radiative Impacts, Journal of the Atmospheric Sciences, https://doi.org/10.1175/1520-0469(2000)057<1841:TASTTC>2.0.CO;2, 2000.

Nakajima, T. and King, M. D.: Determination of the Optical Thickness and Effective Particle Radius of Clouds from Reflected Solar Radiation Measurements. Part I: Theory, Journal of the Atmospheric Sciences, pp. 1878–1893, https://doi.org/10.1175/1520-0469(1990)047<1878:DOTOTA>2.0.CO;2, 1990.

Nakajima, T., King, M. D., Spinhirne, J. D., and Radke, L. F.: Determination of the Optical Thickness and Effective Particle Radius of Clouds from Reflected Solar Radiation Measurements. Part II: Marine Stratocumulus Observations, Journal of Atmospheric Sciences, pp. 728–751, https://doi.org/10.1175/1520-0469(1991)048<0728:DOTOTA>2.0.CO;2, 1991.

https://doi.org/10.5194/egusphere-2025-787
Preprint. Discussion started: 6 March 2025

Ramanathan, V., Cess, R. D., Harrison, E. F., Minnis, P., Barkstrom, B. R., Ahmad, E., and Hartmann, D.: Cloud-Radiative Forcing and Climate: Results from the Earth Radiation Budget Experiment, Science, pp. 57–63, https://doi.org/10.1126/science.243.4887.57, 1989.

Rao, T. N., Sunilkumar, K., and Jayaraman, A.: Validation of humidity profiles obtained from SAPHIR, on-board Megha-Tropiques, CURRENT SCIENCE, 2013.

Rodgers, C. D.: Inverse Methods for Atmospheric Sounding: Theory and Practice, Series on Atmospheric, Oceanic and Planetary Physics, WORLD SCIENTIFIC, ISBN 978-981-02-2740-1 978-981-281-371-8, https://doi.org/10.1142/3171, 2000.

Rosenfeld, D., Cornet, C., Aviad, S., Binet, R., Crebassol, P., Dandini, P., Defer, E., Deschamps, A., Fenouil, L., Frid, A., Holodovsky, V., Kaidar, A., Peroni, R., Pierangelo, C., Price, C., Ricard, D., Schechner, Y., and Yair, Y.: C3IEL: Cluster for Cloud Evolution, ClImatE and Lightning, 2022.

Rosenkranz, P. W.: Retrieval of temperature and moisture profiles from AMSU-A and AMSU-B measurements, IEEE Transactions on Geoscience and Remote Sensing, https://doi.org/10.1109/36.964979, 2001.

Schepers, D., Butz, A., Hu, H., Hasekamp, O. P., Arnold, S. G., Schneider, M., Feist, D. G., Morino, I., Pollard, D., Aben, I., and Landgraf, J.: Methane and carbon dioxide total column retrievals from cloudy GOSAT soundings over the oceans, Journal of Geophysical Research: Atmospheres, https://doi.org/10.1002/2015JD023389, 2016.

Schlüssel, P. and Goldberg, M.: Retrieval of atmospheric temperature and water vapour from IASI measurements in partly cloudy situations, Advances in Space Research, https://doi.org/10.1016/S0273-1177(02)00101-1, 2002.

Schmidt, G. A., Ruedy, R. A., Miller, R. L., and Lacis, A. A.: Attribution of the present-day total greenhouse effect, Journal of Geophysical Research, https://doi.org/10.1029/2010JD014287, 2010.

Schneider, T., O'Gorman, P. A., and Levine, X. J.: WATER VAPOR AND THE DYNAMICS OF CLIMATE CHANGES, Reviews of Geophysics, https://doi.org/10.1029/2009RG000302, 2010.

Sourdeval, O., Labonnote, L. C., Brogniez, G., Jourdan, O., Pelon, J., and Garnier, A.: A variational approach for retrieving ice cloud properties from infrared measurements: application in the context of two IIR validation campaigns, Atmospheric Chemistry and Physics, https://doi.org/10.5194/acp-13-8229-2013, 2013.

Sourdeval, O., C.-Labonnote, L., Baran, A. J., and Brogniez, G.: A methodology for simultaneous retrieval of ice and liquid water cloud properties. Part I: Information content and case study, Quarterly Journal of the Royal Meteorological Society, https://doi.org/10.1002/qj.2405, 2015.

Stocker, T. F., Qin, D., Plattner, G.-K., Tignor, M. M. B., Allen, S. K., Boschung, J., Nauels, A., Xia, Y., Bex, V., and Midgley, P. M., eds.: Climate change 2013: the physical science basis: Working Group I contribution to the Fifth assessment report of the Intergovernmental Panel on Climate Change, Cambridge University Press, ISBN 9781107057999, 2013.

Trenberth, K. E. and Smith, L.: The Mass of the Atmosphere: A Constraint on Global Analyses, Journal of Climate, pp. 864–875, https://doi.org/10.1175/JCLI-3299.1, 2005.

Vesperini, M., Breon, F.-M., and Tanre, D.: Atmospheric Water Vapor Content from Spaceborne POLDER Measurements, IEEE Transactions on Geoscience and Remote Sensing, https://doi.org/10.1109/36.763275, 1999.

Vidot, J., Bennartz, R., O'Dell, C. W., Preusker, R., Lindstrot, R., and Heidinger, A. K.: CO2 Retrieval over Clouds from the OCO Mission: Model Simulations and Error Analysis, Journal of Atmospheric and Oceanic Technology, https://doi.org/10.1175/2009JTECHA1200.1, 2009.

Várnai, T.: Influence of Three-Dimensional Radiative Effects on the Spatial Distribution of Shortwave Cloud Reflection, Journal of the Atmospheric Sciences, pp. 216–229, https://doi.org/10.1175/1520-0469(2000)057<0216:IOTDRE>2.0.CO;2, 2000.

https://doi.org/10.5194/egusphere-2025-787
Preprint. Discussion started: 6 March 2025

Wyser, K.: The Effective Radius in Ice Clouds, Journal of Climate, pp. 1793–1802, https://doi.org/10.1175/1520-0442(1998)011<1793:TERIIC>2.0.CO;2, 1998.